Improved cloud phase retrievals based on remote-sensing observations have the potential to decrease the Southern Ocean shortwave cloud radiation bias

W. Schimmel[1,2], C. Barrientos-Velasco [2], J. Witthuhn[1,2], M. Radenz [2], B. Barja González [3], and H. Kalesse-Los[1]

[1]Leipzig Institute for Meteorology, University of Leipzig, Leipzig, Germany
[2]Leibniz Institute for Tropospheric Research (TROPOS), Leipzig, Germany
[3]Atmospheric Research Laboratory, University of Magallanes, Punta Arenas, Chile

Key Points:

- Southern Ocean radiative closure study shows potential of reducing shortwave radiation bias using machine-learning cloud liquid retrieval.

Corresponding author: Willi Schimmel, willi.schimmel@uni-leipzig.de

Abstract

Accurately identifying liquid water layers in mixed-phase clouds is crucial for estimating cloud radiative effects. Lidar-based retrievals are limited in optically thick or multilayer clouds, leading to positive biases in simulated shortwave radiative fluxes. At the same time, general circulation models also tend to overestimate the downwelling shortwave radiation at the surface especially in the Southern Ocean regions. To reduce this SW radiation bias in models, we first need better observational-based retrievals for liquid detection which can later be used for model validation. To address this, a machine-learning-based liquid-layer detection method called VOODOO was employed in a proof-of-concept study using a single column radiative transfer model to compare shortwave cloud radiative effects of liquid-containing clouds detected by Cloudnet and VOODOO to ground-based and satellite observations. Results showed a reduction in shortwave radiation bias, indicating that liquid-layer detection with machine-learning retrievals can improve radiative transfer simulations.

Plain Language Summary

This article discusses the challenges of accurately identifying liquid water layers within mixed-phase clouds, which is important for understanding precipitation formation and estimating cloud radiative effects. While remote-sensing retrievals using lidar can be useful for this purpose, they are limited in optically thick or multilayer clouds, leading to biases in simulated radiative fluxes. The authors propose a machine-learning-based method called VOODOO to better detect supercooled-liquid in clouds, which can help reduce biases in radiative transfer simulations and improve model validation. A proof-of-concept study was conducted using a single column radiative transfer calculation, comparing shortwave cloud radiative effects of liquid-containing clouds detected by Cloudnet and VOODOO to ground-based and satellite observations. Results showed a reduction in shortwave radiation bias, suggesting that liquid-layer detection with machine-learning retrievals can improve radiative transfer simulations.

1 Introduction

Supercooled liquid water clouds and mixed-phase clouds are common over the Southern Ocean (Hu et al., 2010; Kanitz et al., 2011; Morrison et al., 2011; Huang et al., 2012; Radenz et al., 2021). Only a few long-term observations are available from the southern mid-latitudes, and most of them are either based on lidar-only (Kanitz et al., 2011), space-borne radar-lidar datasets with limited sensitivity (Zhang et al., 2010; Wang et al., 2016), or short-term ship-based measurements (Gettelman et al., 2020; Mace et al., 2021; Xi et al., 2022). The lack of long-term ground-based remote-sensing observations of the atmosphere in this region motivated the long-term Dynamics Aerosol Clouds And Precipitation Observation in the Pristine Environment of the Southern Ocean (DACAPO-PESO) field campaign in Punta Arenas (53.13° S, 70.88° W), Chile, which resulted e.g., in an in-depth analysis of shallow mixed-phase clouds by Radenz et al. (2021). Mixed-phase clouds are difficult to represent in global climate models (GCM), which is problematic because, as e.g. Gregory and Morris (1996) and Li and Treut (1992) showed, modelled variables such as cloud cover, cloud albedo, outgoing terrestrial (longwave) radiation, and cloud water content depend significantly on the temperature range in which liquid water and ice are assumed to coexist. To date, large uncertainties remain in the representation of mixed-phase clouds in GCM (McCoy et al., 2016). Comparisons of various GCMs predict vastly different distributions of thermodynamic cloud phase for a given temperature, where none of them are capable of reproducing the observations in spatial distribution nor magnitude (Bony et al., 2006; Grise & Polvani, 2014a; Grise et al., 2015). Also, Komurcu et al. (2014) suggested that validating GCMs using only the vertically

integrated water contents could lead to amplified differences in cloud radiative feedback. The Southern Ocean region is associated with significant uncertainties in estimates of cloud properties in GCMs. In this region, the amount of supercooled liquid water in clouds is underestimated, causing shortwave (SW) radiative flux biases (Kay et al., 2016; Bodas-Salcedo et al., 2016; Gettelman et al., 2020). Also, the use of reanalysis products with wrong cloud phases in GCM (Naud et al., 2014) have been attributed to the inability of models to represent the frequency of occurrence of supercooled water in mixed-phase volumes. Even if models estimate the correct total condensed water content, the same amount of condensed water in the ice phase results in a lower cloud albedo compared to the liquid phase. This is because the ice particles are smaller in number but larger in size than the corresponding liquid droplets, so the optical thickness of the glaciated cloud is smaller. Therefore, the identification of the spatial distribution of liquid droplets in mixed-phase clouds is of great importance not only because the radiative properties of water and ice are different (Sun & Shine, 1994) but also because they influence the formation of precipitation (Field & Heymsfield, 2015; Mülmenstädt et al., 2015) and thus ultimately cloud lifetime. Synergistic remote-sensing observations of clouds and the ongoing development of retrievals of microphysical cloud properties - such as cloud thermodynamic phase - continue to enhance the understanding of MPC process (Shupe et al., 2005; Bühl et al., 2016; Mace & Protat, 2018; Griesche et al., 2020; Zaremba et al., 2020). Accurate retrievals of cloud thermodynamic phase are required for constraining cloud phase representation in GCM (Fiddes et al., 2022). Several studies showed that the shortwave radiative transfer, especially through mixed-phase clouds, depends highly on the amount and location of liquid cloud droplets (McFarquhar et al., 2021; Barrientos-Velasco et al., 2022). An underestimation in the liquid water-path (LWP) leads to a less radiative opaque cloud, which subsequently leads to an underestimation of the cloud radiative effect at the surface (Cesana & Storelvmo, 2017; Tan & Storelvmo, 2019).

The question we are addressing in this study is if and to what extent improved cloud phase retrievals from ground-based remote sensing observations can reduce the SW radiation bias in the Southern Ocean. We introduce the data set in Section 2 and explain how the improved cloud phase detection algorithm VOODOO works in Section 3. The radiative transfer simulation architecture is also described in Section 3. Results of radiative flux comparison are shown in Section 4 to evaluate the concept. The study ends with discussions and conclusions in Section 5.

2 Datasets

2.1 Ground-based remote sensing dataset

The core instrumentation used for this work is provided by the Leipzig Institute for Meteorology (LIM) and the Leibniz Institute for Tropospheric Research (TROPOS). Specifically, the five data sources considered are the following:

1. Profiles of cloud radar Doppler spectra and moments from the RPG-FMCW94-DP, a frequency modulated continuous wave 94 GHz vertically-pointing Doppler cloud radar with polarimetric capabilities (Küchler et al., 2017),
2. Profiles of attenuated backscatter coefficient β_{att} from the Jenoptik CHM15kx, a 1064 nm ceilometer (Heese et al., 2010),
3. Liquid water path (LWP) retrieved from the RPG-HATPRO-G2, a 14-channel microwave radiometer (MWR; Rose et al. (2005)),
4. Temperature, relative humidity and pressure from the European Centre for Medium-Range Weather Forecasts integrated forecasting system (ECMWF-IFS; "ECMWF Forecast User Guide" (2018)),
5. Shortwave downward irradiance from the TROPOS *Mobile Radiation Observatory (MORDOR)* (2022), measured with a Class A pyranometer (ISO 9060:2018,

2018) of the type MS-80, from the manufacturer EKO Instruments, with measurement uncertainty under clear sky conditions of about 2 %.

The classical Cloudnet multi-sensor approach by Illingworth et al. (2007) converts the information of 1.–4. into an atmospheric target classification and higher level microphysical products such as ice and liquid water contents (IWC and LWC) and the respective ice crystal and droplet effective radii ($r_{\text{eff}}^{\text{ice}}$ and $r_{\text{eff}}^{\text{liq}}$). In this work, we use the latest implementation of CloudnetPy (Tukiainen et al., 2020). A detailed description of instruments and parameters is presented in Schimmel et al. (2022). The latter data source (5.) is considered for the validation of the shortwave radiative transfer simulations at the surface.

2.2 Ancillary dataset

The data sets used as input parameters for the radiative transfer simulations are based on the hourly pressure level profiles of temperature, pressure, ozone mass mixing ratio and specific humidity from the European Centre for Medium-Range Weather Forecasts (ECMWF) Re-Analysis (ERA5), and single levels of surface pressure and skin temperature (Hersbach et al., 2020). The ERA5 dataset has a spatial grid from 0.25° latitude by 0.25° longitude. We opted for this dataset due its consistency and realistic representation of the atmospheric conditions as described in previous studies (Goyal et al., 2021; Hoffmann & Spang, 2022). The surface albedo used for the radiative transfer simulations is based on CERES (Clouds and the Earth's Radiant Energy System) Synoptic 1-degree daily flux (SYN1deg, ed.4) products (Minnis et al. (2021); hereafter CERES SYN), which has been collocated to the location of the remote sensing station in Punta Arenas, Chile. The atmospheric trace gases quantities were obtained from the climatological values from the Air Force Geophysics Laboratory (AFGL) for a mid-latitude summer atmosphere (Anderson et al., 1986). The CERES SYN parameters are provided in a spatial resolution of 1° latitude by 1° longitude and at a 1 hour temporal resolution. The mentioned ancillary data products were collocated and linearly interpolated in time to the location and time of interest.

3 Methodology

The following section describes the methods to retrieve the cloud macro- and microphysical properties used to generate the input data for the radiative transfer simulations (RTS) and then the RTS framework used to simulate the shortwave irradiances and the derivation of the cloud radiative effects.

3.1 Description of Cloudnet and VOODOO

This section introduces the methods to retrieve the thermodynamic phase of clouds using ground-based remote sensing observations of MPCs and the distribution of liquid and ice. As reference simulation we use the products of the CloudnetPy toolbox (Tukiainen et al., 2020), which provides cloud properties such as IWC, LWC, $r_{\text{eff}}^{\text{ice}}$, and $r_{\text{eff}}^{\text{liq}}$. CloudnetPy is able to distinguish between different hydrometeor types such as drizzle/rain, ice, melting layer, liquid droplets, and mixed-phase (ice + liquid droplets). However, the identification of liquid droplets relies entirely on the attenuated backscatter coefficient β_{att} of the lidar, which is quickly attenuated by liquid layers. For this reason, the liquid droplet detection of CloudnetPy beyond full lidar attenuation is not reliable, limiting the application to thin, single layer stratiform clouds. The new machine learning approach by Schimmel et al. (2022) is used as add-on to CloudnetPy, for reVealing supercOOled liquiD layers beyOnd lidar attenuatiOn (VOODOO). The VOODOO algorithm is based on a convolutional neural network. The radar Doppler spectra (image) is processed into likelihood for the presence of (supercooled) liquid cloud droplets. How-

ever, due to the lower sensitivity of the Doppler cloud radar to liquid droplets (compared to lidar), small droplet number concentrations, or thin liquid layers of small droplets are not visible to the Doppler radar. Thus, liquid cloud droplet predictions By VOODOO are used to augment the Cloudnet atmospheric target classification in altitudes where no valid lidar signal (due to complete lidar signal attenuation) is received. Clearly, Cloudnet's lidar-based approach has an advantage in detecting even thin liquid water layers, whereas VOODOO's radar approach can be used primarily to reveal liquid water layers beyond lidar attenuation in multi-layer or deep MPC. Both approaches complement each other perfectly and are now available as Cloudnet product in the latest Python-based GitHub release `github.com/actris-cloudnet/cloudnetpy`. The VOODOO method is also available as stand-alone version `github.com/actris-cloudnet/voodoonet`.

3.2 Description of T-CARS

The radiative transfer simulations were carried out using the TROPOS – Cloud and Aerosol Radiative effect Simulator (hereafter T-CARS). T-CARS is a Python-based environment created to conduct radiative transfer simulations with a particular focus on the investigation of the radiative effects of aerosols, and clouds (Barlakas et al., 2020; Witthuhn et al., 2021; Barrientos-Velasco et al., 2022). The radiative transfer solver used was a 1D single column rapid radiative transfer model (RRTM) for GCM applications (RRTMG; Mlawer et al. (1997); Barker et al. (2003); Clough et al. (2005)). T-CARS output files have a standard atmospheric grid that consists of 197 levels ranging from the surface up to 20 km height at 1-minute temporal resolution, as described in Barrientos-Velasco et al. (2022) and published on Zenodo (Barrientos-Velasco, 2023). The first 10 km of the atmosphere is divided into 160 levels with a geometric layer thickness of about 62.5 m. The level thickness of each pixel for the first 10 km of the atmosphere corresponds to two vertical levels of Cloudnet pixels, which are averaged to the standard grid. The T-CARS output files provide simulated clear-sky and all-sky atmospheric profiles of broadband longwave (LW) and SW radiative fluxes and heating rates. We focus on the SW broadband flux by calculating the flux difference between simulated and observed radiative fluxes, describing heating rates and computing the SW cloud radiative effect (CRE) following Eq. 1 and 2.

$$CRE_{SW,BOA} = (F^{\downarrow}_{SW} - F^{\uparrow}_{SW})_{all-sky} - (F^{\downarrow}_{SW} - F^{\uparrow}_{SW})_{clear-sky}. \quad (1)$$

$$CRE_{SW,TOA} = (F^{\uparrow}_{SW})_{clear-sky} - (F^{\uparrow}_{SW})_{all-sky}. \quad (2)$$

4 Results

The results are presented in two subsections. First, a description of the cloud microphysical retrievals of Cloudnet and the improved retrieval VOODOO is given. The second subsection compares the radiative simulation results based on Cloudnet alone and VOODOO+Cloudnet input by comparing the bottom-of-atmosphere (BOA) shortwave downwelling (SWD) radiative fluxes as well as the simulated upward SW flux (SWU) at the top-of-the atmosphere (TOA) with CERES SYN observations. Moreover, the shortwave CRE, and SW heating rate are calculated. Note that the simulations based on Cloudnet are referred to as Cloudnet-Sim (CSim), and the simulations based on the enhancement of the Cloudnet liquid detection by VOODOO are referred to as VOODOO-Cloudnet-Sim (VCSim). However, for simplicity the latter is labelled as Cloudnet and VOODOO results, respectively in Table 1, Fig. 3, Fig. 3, and Fig. 4.

4.1 Cloud microphysical retrieval results

The focus of this analysis is to quantify the effect of the improved thermodynamic phase classification by VOODOO (Schimmel et al., 2022) compared to the reference retrieval Cloudnet (Illingworth et al., 2007; Tukiainen et al., 2020).

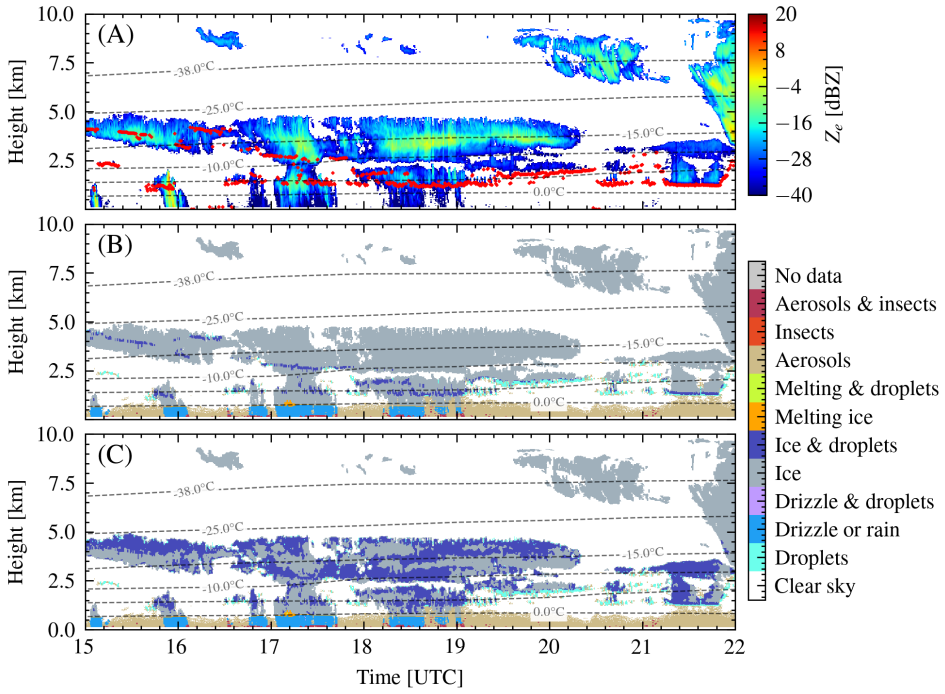

Figure 1. Cloud situation on 2 January 2019 in Punta Arenas, Chile. (A) Radar reflectivity Z_e, (B) atmospheric target classification of Cloudnet, and (C) combination of atmospheric target classification of Cloudnet enhanced by the liquid predictions of VOODOO. Dashed lines depict the isotherm lines from ECMWF temperature profiles. The red dots in (A) indicate the ceilometer cloud base height.

In this study, the focus is on the period between 15:00–22:00 UTC on 2 January 2019 in Punta Arenas Chile, when multilayer MPC were observed. Figure 1 (A) shows the radar reflectivity factor Z_e, and the target classification of Cloudnet (B) and VOODOO (C). Multiple showers of very low precipitation intensity were observed by the radar in the first half of the case study. However, no precipitation was measured by ground-based in-situ rain sensors. The ceilometer cloud base height shown by red dots in Fig. 1 (A) indicates the first supercooled liquid layer height, which matches the liquid detections (classes: 'Droplets' and 'Ice & droplets') in the Cloudnet target classification (B). However, Cloudnet detects only the first liquid cloud base layer, while VOODOO reveals additional supercooled liquid layers in altitudes between 2.5–5.0 km with cloud top temperatures down to $T = -25°$ C. Parts of the required input parameters for the radiative transfer simulations are the IWC and LWC as shown in Fig. 2. The IWC (A) is equal for Cloudnet and VOODOO, with values ranging from 10^{-5} to $2{\times}10^{-4}\,\mathrm{kg\,m^{-3}}$. However, differences in the distribution of the liquid layers within the observed clouds are clearly visible in Fig. 2 (B), (C) and Fig. 4 (A). The scaling approach used in Cloudnet processing, distributes all the liquid water detected by the MWR into thin liquid layers (with depths < 150 m), resulting in Cloudnet mean LWC values of $3{\times}10^{-3}\,\mathrm{kg\,m^{-3}}$. By using of VOODOO+Cloudnet liquid detection, the LWC is distributed over a greater liquid layer depth, reaching mean LWC values of $5 \times 10^{-4}\,\mathrm{kg\,m^{-3}}$.

4.2 Analysis of simulated SW radiative fluxes and heating rates

Radiative transfer simulations were performed to evaluate the radiative effect of the different cloud microphysical properties from CSim and VCSim parameterizations.

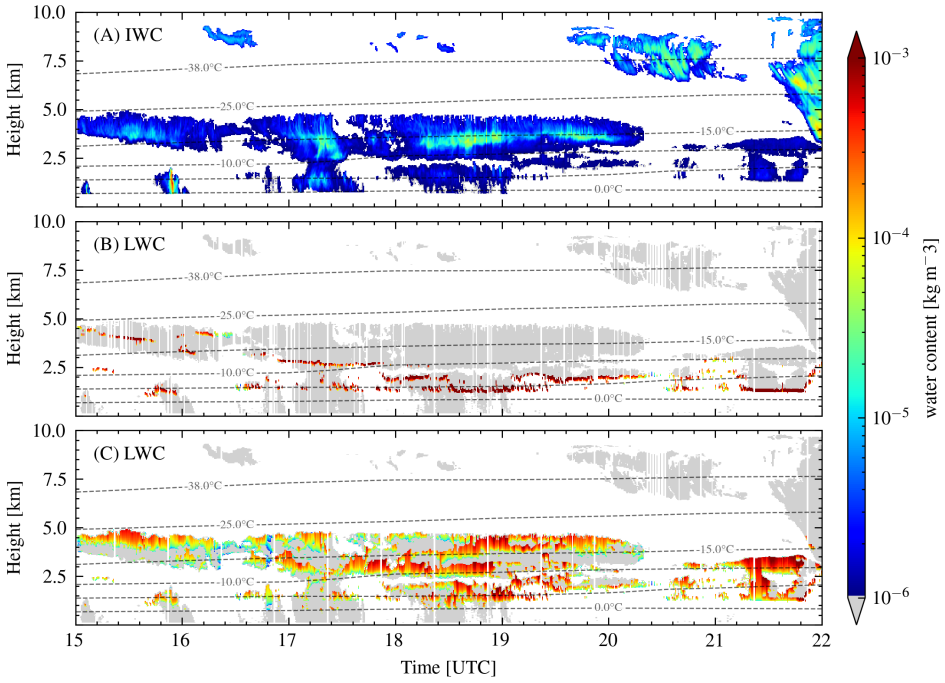

Figure 2. Panel (A) shows ice water content of both, Cloudnet and VOODOO, for 2 January 2019 in Punta Arenas, Chile. (B) Cloudnet liquid water content, and (C) Cloudnet liquid water content enhanced by liquid predictions of VOODOO. In (B) and (C), colored pixels reflect liquid-bearing cloud volumes and grey pixels other hydrometeor types (see Fig. 1). Dashed lines depict the isotherm lines from ECMWF temperature profiles.

The analysis focuses on comparing the SWU at the TOA (Fig. 3 A and B), SWD at BOA (Fig. 3 C and D), and the atmospheric SW heating rates (Fig. 4). The results are summarized in Table 1. Additionally, the comparison differentiates the periods when the cloud cover was homogeneous or inhomogeneous, which is important to keep in mind when comparing observations of pencil-beam radar-lidar measurements to all-sky pyranometer measurements. At the TOA, the simulated fluxes are compared to the collocated CERES SYN observations (Fig. 3 A and B). The values from CERES SYN indicate a semi-continuous SWU flux between 300 to 600 W m^{-2} while the T-CARS radiative transfer simulations range from 100 to 800 W m^{-2} (Fig. 3A). Given that the surface albedo used for the simulations is from CERES SYN, the observed differences of more than 100 W m^{-2} at the TOA indicate a plausible overestimation of the cloud top albedo due to a large amount of the water content in the cloud or small particle sizes (Vergara-Temprado et al., 2018). However, it should be noted that the difference in spatial resolution might also play a role in the flux differences since the spatial grid of CERES SYN is of 1° by 1° and the simulations are focused on a point measurement at Punta Arenas with a contrasting water/land surface conditions near the Strait of Magellan that adds complexity to the system. Despite these differences, the results indicate a better agreement between VOODOO-based radiative transfer simulations than for Cloudnet-only for the SWU flux with an improvement in the correlation coefficients (r^2) and a decrease of the mean-absolute-error (MAE) and root-mean-squared-error (RMSE) of 15–20 % for both inhomogeneous and homogeneous atmospheres (Table 1). The time series of the CRE$_{SW,TOA}$ is shown in Fig d3 B. For homogeneous cloud conditions, the mean CRE$_{SW,TOA}$ are -362, -254, -428 W m^{-2} for CERES SYN, CSim and VCSim, respectively. The values indicate a better agreement between VCSim and the CERES SYN observations at the TOA. The significant differ-

Table 1. Table of time-series mean values (Mean) in $\mathrm{W\,m^{-2}}$, correlation coefficient (r^2), root mean squared error (RMSE) in $\mathrm{W\,m^{-2}}$, mean absolute error (MAE) in $\mathrm{W\,m^{-2}}$, of pyranometer (BOA) and CERES SYN (TOA) observations (O), as well as T–CARS simulations of TOA-SWU, BOA-SWD radiation fluxes, $\mathrm{CRE}_{SW,TOA}$ and $\mathrm{CRE}_{SW,BOA}$ using Cloudnet (C) or VOODOO-Cloudnet (VC) as input case study on 2 January 2019 in Punta Arenas, Chile. Results are presented for the entire time period of 15:00 - 22:00 UTC ("inhom") and for stratiform cloud conditions only excluding broken cloud situations ("hom").

		Mean	r^2	RMSE	MAE
		O / C / VC	C / VC	C / VC	C / VC
TOA-SWU	inhom.	481 / 354 / 543	0.35 / 0.62	237 / 189	210 / 169
	hom.	440 / 378 / 553	0.33 / 0.81	204 / 164	166 / 142
$\mathrm{CRE}_{SW,TOA}$	inhom.	−398 / −218 / −406	0.29 / 0.58	271 / 177	236 / 150
	hom.	−362 / −254 / −428	0.19 / 0.75	229 / 133	179 / 110
BOA-SWD	inhom.	274 / 564 / 349	0.53 / 0.73	381 / 180	315 / 125
	hom.	191 / 432 / 234	0.50 / 0.77	345 / 126	251 / 74
$\mathrm{CRE}_{SW,BOA}$	inhom.	−511 / −247 / −437	0.42 / 0.70	348 / 177	290 / 124
	hom.	−499 / −281 / −457	0.32 / 0.79	313 / 126	229 / 74

ences between Cloudnet and observations estimations are due to the underestimation of the liquid water content in the cloud layer. For inhomogeneous conditions, the mean $\mathrm{CRE}_{SW,TOA}$ for CERES SYN, CSim, and VCSim are -398, -218, -406 $\mathrm{W\,m^{-2}}$, respectively (see Table 1). The differences are larger due to the limitations of the representations of these types of clouds in a single column 1D radiative transfer simulations and the different spatial representations between CERES SYN and the point measurements of the remote sensing instrumentation. The comparison between simulated and observed SWD fluxes at the BOA, as shown in Fig. 3 C, indicates that the simulations agree better with the observations when using VOODOO-based input compared to Cloudnet-only input. The results for VCSim simulations show that the mean absolute SWD radiation bias is reduced by 70 % when the cloud cover is homogeneous. During broken cloud conditions, the differences are also reduced in VCSim, but to a lesser extent. However, it should be noted that during these conditions, 1D radiative transfer simulations cannot resolve broken cloud conditions well, and more complex methods, such as 3D radiative transfer models, should be applied. The latter is beyond the scope of this study. Panel D in Fig. 3 shows the time series of the calculated $\mathrm{CRE}_{SW,BOA}$ for CSim and VCSim and a calculation substituting the simulated all-sky SWD flux with observations from the downwelling pyranometer. The CRE_{SW} results show a good agreement between VCSim and the calculations considering the observations with correlation coefficients above 0.7 for both homogeneous and inhomogeneous cloud conditions. The positive $\mathrm{CRE}_{SW,BOA}$ derived from pyranometer observations shown at around 15:00 and 16:30 UTC is due to the multiple scattering in broken cloud conditions leading to larger SWD values than during clear-sky conditions (Schade et al., 2007). The VCSim results indicate a reduction of the mean absolute error by 68 %. The mean CRE_{SW} percentage error between CSim and the pyranometer observations is 44 %, while the VCSim reduce the error to 8 % (see Table 1). The radiative heating rates (SWHR) are calculated for VCSim input and CSim simulation input to determine the change in the net SW flux in the atmospheric profile. The results show the dependency of the SW heating effect on the location of the liquid layer (see Fig. 4). The VCSim distribution of the liquid layers up to an altitude around 4.5 km leads to an important cloud top warming of up to 12 K $\mathrm{day^{-1}}$ suppressing the warming in the lower atmosphere since part of this radiation is reflected upward. In contrast,

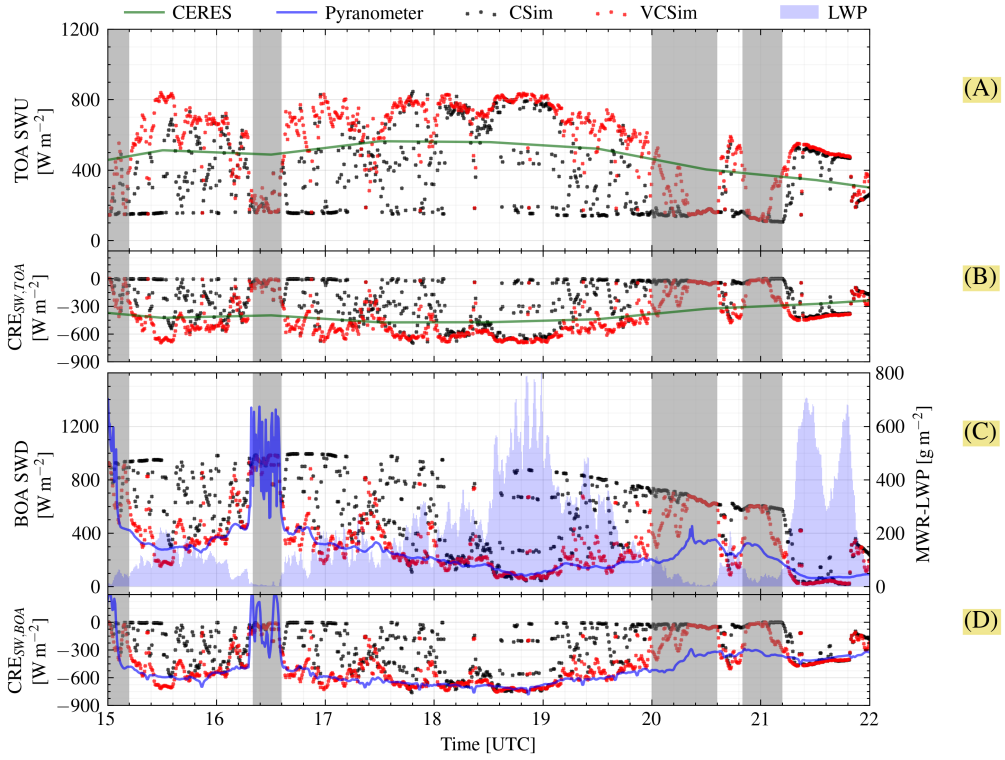

Figure 3. (A) Time series of top-of-atmosphere shortwave upwelling irradiance simulations for Cloudnet (black dots), VOODOO+Cloudnet (red dots), and CERES SYN observations (green line). (B) Time series of the top-of-atmosphere cloud radiative effect (CRE) based on simulated fluxes for Cloudnet (black dots) and VOODOO+Cloudnet (red dots). The grey background band flags broken cloud situations. (C) Time series of bottom-of-atmosphere (BOA) shortwave downwelling irradiance simulations and pyranometer observations (blue line, left y-axis), simulations (black and red dots, left y-axis) and MWR-LWP (blue bars, right y-axis). (D) Time series of the bottom-of-atmosphere cloud radiative effect based on simulated fluxes for Cloudnet (black dots) and VOODOO+Cloudnet (red dots).

CSim based simulations show the most significant cloud opacity at around 1.5 km leading to a SWHR of about $9\,\mathrm{K\,day^{-1}}$ at this height. In general, there are no significant changes in the mean SWHR between homogeneous and inhomogeneous cloud conditions. The small changes observed in Fig. 4B are due to an increase in the LWC when considering homogeneous clouds only, as detailed in Fig. 4A. It is worth noting that the clear-sky (CS) profiles, shown in solid black line, show slightly positive SWHR due to the enhanced water vapour at the heights of the cloud.

5 Discussions, Conclusions and Outlook

The presented study shows the potential of the novel cloud liquid detection machine learning method VOODOO in reducing SW flux biases. Our study focuses on a multilayer mixed-phase cloud case study in the Southern Hemisphere in Punta Arenas, Chile. The approach consists in improving the multi-sensor products (LWC, IWC, $r_{\mathrm{eff}}^{\mathrm{ice}}$ and $r_{\mathrm{eff}}^{\mathrm{liq}}$) of Cloudnet by using VOODOO. Single column 1D radiative transter simulations were performed to test the applicability of VOODOO and Cloudnet and quantify

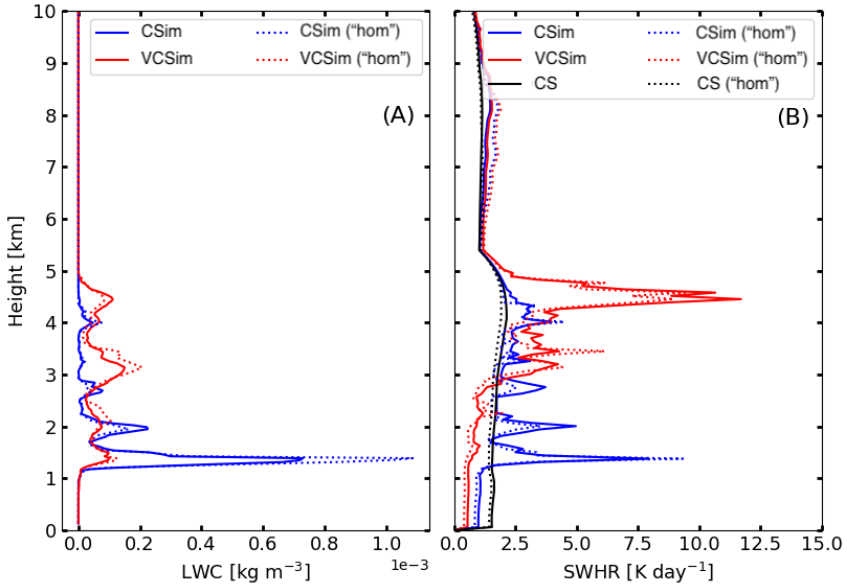

Figure 4. Mean profiles of liquid water content (LWC) in (A) and shortwave atmospheric heating rate (SWHR) for all-sky conditions for Cloudnet (blue line), VOODOO-Cloudnet (red line), and clear-sky (CS; black line) in panel (B). Solid lines show SWHR for the entire period 15:00–22:00 UTC on 2 January 2019 and dotted line for homogeneous clouds ("hom") only.

the differences in radiative fluxes at the TOA, atmosphere and BOA. Based on the observational availability of ground-based radiation measurements, we focus on the broadband SW flux and summarize the findings in the following bullet points:

- The analysis of the simulations indicate that the VOODOO-based method decreases RMSE and MAE values at the TOA up to 20 % and at the BOA up to 70 %, suggesting an improvement to the use of Cloudnet retrievals alone. While biases are reduced in both TOA and BOA, the results also indicate larger values of the SWU flux at the TOA from VCSim than CERES SYN values most likely attributed to the different spatial scale of a complex surface albedo as it also discussed in a relatively similar comparison for the Southern Hemisphere in the Tropical Western Pacific site at Darwin (TWPC3) in Dolinar et al. (2016). The analysis at TOA is as important as at BOA as it constitutes a reference of the absorbed SW radiation by the surface and atmosphere, which still is part of the large model uncertainties reported in previous studies (Bodas-Salcedo et al., 2016; Kay et al., 2016).
- The analysis of the CRE_{SW} shows a prominent cooling effect at the BOA and the TOA. At the TOA and BOA, the results are consistent with Haynes et al. (2011) and Grise and Polvani (2014b), who report large values of CRE_{SW} for the location of Punta Arenas during summer based on satellite observations and model evaluations. It should be noted, however, that their results are averaged for a more extended period and area of analysis. The large instantaneous CRE_{SW} values presented in this study are dominated by the effect of supercooled liquid droplets as it is characteristic of the region of analysis as discussed in Bodas-Salcedo et al. (2016).
- The comparison of SWHR revealed a relevant difference in the warming SW effect height that explained the SWU flux difference between VCSim and CSim at the TOA. The latter emphasizes the importance of correctly retrieving the distribution of liquid water content within the clouds since the effect on radiation is of particular interest in stratiform clouds when the atmospheric radiation plays

a more relevant role in the diabatic heating of the atmosphere, which can potentially perturb the local atmospheric stability (Turner et al., 2018).

The presented case study details the promising use of VOODOO to reduce software biases caused by the misclassification of cloud thermodynamic phase and the consequent misidentification of the location of LWC in the atmospheric column. This technique could potentially be used in other cases of mixed-phase clouds where similar challenges have been previously described (Barrientos-Velasco et al., 2022; Fiddes et al., 2022). Additionally, there is an envisioned plan to study more cases from the three-year DACAPO-PESO campaign, as well as other cases from the ARM Southern Ocean MARCUS shipborne field campaign (Xi et al., 2022). However, future studies should also consider the effect of longwave radiative flux. Moreover, there is a plan to test the VOODOO-based method on future long-term Southern Ocean deployments of the Leipzig Aerosol and Cloud Remote Observations System (LACROS) station on the South Island of New Zealand.

Acknowledgments

This research has been supported by the Federal State of Saxony and the European Social Fund (ESF) in the framework of the programme "Projects in the fields of higher education and research" (grant no. 100339509) and ESF-REACT (grant no. 100602743). We gratefully acknowledge the Bundesministerium für Bildung und Forschung for the project "Combining MOSAiC and Satellite Observations for Radiative Closure and Climate Implications" (MOSaRiCs) – Project Number 03F0890A. We acknowledge the National Fund for Scientific and Technological Development of Chile, FONDECYT, through grant agreement No. 11181335.

6 Data Availability Statement

The Cloudnet products and VOODOO enhanced data files are available at Zenodo via `https://doi.org/10.5281/zenodo.7760395` (Schimmel, 2023) The radiative transfer simulations data files generated in this study are available at Zenodo via `https://doi.org/10.5281/zenodo.7674862` (Barrientos-Velasco, 2023). The CERES SYN1deg Ed.4.1 data used for the surface albedo and all-sky and clear sky broadband upward shortwave radiative fluxes at the TOA are available at NASA Langley Research Center Atmospheric Science Data Center via `10.5067/Terra+Aqua/CERES/SYN1deg-1Hour_L3.004A`.

References

Anderson, G. P., Clough, S. A., Kneizys, F. X., Chetwynd, J. H., & Shettle, E. P. (1986, 05). Afgl (air force geophysical laboratory) atmospheric constituent profiles (0. 120km). environmental research papers. , 46. Retrieved from `https://www.osti.gov/biblio/6862535`

Barker, H. W., Stephens, G. L., Partain, P. T., Bergman, J. W., Bonnel, B., Campana, K., ... Yang, F. (2003). Assessing 1d atmospheric solar radiative transfer models: Interpretation and handling of unresolved clouds. *Journal of Climate*, *16*(16), 2676 - 2699. Retrieved from `https://journals.ametsoc.org/view/journals/clim/16/16/1520-0442_2003_016_2676_adasrt_2.0.co_2.xml` doi: 10.1175/1520-0442(2003)016⟨2676:ADASRT⟩2.0.CO;2

Barlakas, V., Deneke, H., & Macke, A. (2020). The sub-adiabatic model as a concept for evaluating the representation and radiative effects of low-level clouds in a high-resolution atmospheric model. *Atmospheric Chemistry and Physics*, *20*(1), 303–322. Retrieved from `https://acp.copernicus.org/articles/20/303/2020/` doi: 10.5194/acp-20-303-2020

Barrientos-Velasco, C. (2023, March). *Single column 1D radiative transfer simu-*

lations for a case study of low-level-stratus clouds in the central Arctic during PS106. Zenodo. Retrieved from https://doi.org/10.5281/zenodo.7674862 doi: 10.5281/zenodo.7674862

Barrientos-Velasco, C., Deneke, H., Hünerbein, A., Griesche, H. J., Seifert, P., & Macke, A. (2022). Radiative closure and cloud effects on the radiation budget based on satellite and shipborne observations during the arctic summer research cruise, ps106. *Atmospheric Chemistry and Physics*, *22*(14), 9313–9348. Retrieved from https://acp.copernicus.org/articles/22/9313/2022/ doi: 10.5194/acp-22-9313-2022

Bodas-Salcedo, A., Hill, P. G., Furtado, K., Williams, K. D., Field, P. R., Manners, J. C., ... Kato, S. (2016). Large contribution of supercooled liquid clouds to the solar radiation budget of the southern ocean. *Journal of Climate*, *29*(11), 4213 - 4228. Retrieved from https://journals.ametsoc.org/view/journals/clim/29/11/jcli-d-15-0564.1.xml doi: 10.1175/JCLI-D-15-0564.1

Bony, S., Colman, R., Kattsov, V. M., Allan, R. P., Bretherton, C. S., Dufresne, J.-L., ... Webb, M. J. (2006). How well do we understand and evaluate climate change feedback processes? *Journal of Climate*, *19*(15), 3445 - 3482. Retrieved from https://journals.ametsoc.org/view/journals/clim/19/15/jcli3819.1.xml doi: 10.1175/JCLI3819.1

Bühl, J., Seifert, P., Myagkov, A., & Ansmann, A. (2016). Measuring ice- and liquid-water properties in mixed-phase cloud layers at the leipzig cloudnet station. *Atmospheric Chemistry and Physics*, *16*(16), 10609–10620. Retrieved from https://acp.copernicus.org/articles/16/10609/2016/ doi: 10.5194/acp-16-10609-2016

Cesana, G., & Storelvmo, T. (2017). Improving climate projections by understanding how cloud phase affects radiation. *Journal of Geophysical Research: Atmospheres*, *122*(8), 4594-4599. Retrieved from https://agupubs.onlinelibrary.wiley.com/doi/abs/10.1002/2017JD026927 doi: 10.1002/2017JD026927

Clough, S., Shephard, M., Mlawer, E., Delamere, J., Iacono, M., Cady-Pereira, K., ... Brown, P. (2005). Atmospheric radiative transfer modeling: a summary of the aer codes. *Journal of Quantitative Spectroscopy and Radiative Transfer*, *91*(2), 233-244. Retrieved from https://www.sciencedirect.com/science/article/pii/S0022407304002158 doi: https://doi.org/10.1016/j.jqsrt.2004.05.058

Dolinar, E. K., Dong, X., Xi, B., Jiang, J. H., & Loeb, N. G. (2016). A clear-sky radiation closure study using a one-dimensional radiative transfer model and collocated satellite-surface-reanalysis data sets. *Journal of Geophysical Research: Atmospheres*, *121*(22), 13,698-13,714. Retrieved from https://agupubs.onlinelibrary.wiley.com/doi/abs/10.1002/2016JD025823 doi: https://doi.org/10.1002/2016JD025823

Ecmwf forecast user guide. (2018, 05). , *2018*. Retrieved from https://www.ecmwf.int/node/16559 doi: 10.21957/m1cs7h

Fiddes, S. L., Protat, A., Mallet, M. D., Alexander, S. P., & Woodhouse, M. T. (2022). Southern ocean cloud and shortwave radiation biases in a nudged climate model simulation: does the model ever get it right? *Atmospheric Chemistry and Physics*, *22*(22), 14603–14630. Retrieved from https://acp.copernicus.org/articles/22/14603/2022/ doi: 10.5194/acp-22-14603-2022

Field, P. R., & Heymsfield, A. J. (2015). Importance of snow to global precipitation. *Geophysical Research Letters*, *42*(21), 9512-9520. Retrieved from https://agupubs.onlinelibrary.wiley.com/doi/abs/10.1002/2015GL065497 doi: https://doi.org/10.1002/2015GL065497

Gettelman, A., Bardeen, C. G., McCluskey, C. S., Järvinen, E., Stith, J., Bretherton, C., ... Wu, W. (2020). Simulating observations of southern

ocean clouds and implications for climate. *Journal of Geophysical Research: Atmospheres*, *125*(21), e2020JD032619. Retrieved from https://agupubs.onlinelibrary.wiley.com/doi/abs/10.1029/2020JD032619 (e2020JD032619 10.1029/2020JD032619) doi: https://doi.org/10.1029/2020JD032619

Goyal, R., Sen Gupta, A., Jucker, M., & England, M. H. (2021). Historical and projected changes in the southern hemisphere surface westerlies. *Geophysical Research Letters*, *48*(4), e2020GL090849. Retrieved from https://agupubs.onlinelibrary.wiley.com/doi/abs/10.1029/2020GL090849 (e2020GL090849 2020GL090849) doi: https://doi.org/10.1029/2020GL090849

Gregory, D., & Morris, D. (1996). The sensitivity of climate simulations to the specification of mixed-phase clouds. *Climate Dyn.*, *12*, 641–651.

Griesche, H. J., Seifert, P., Ansmann, A., Baars, H., Barrientos Velasco, C., Bühl, J., ... Macke, A. (2020). Application of the shipborne remote sensing supersite oceanet for profiling of arctic aerosols and clouds during polarstern cruise ps106. *Atmospheric Measurement Techniques*, *13*(10), 5335–5358. Retrieved from https://amt.copernicus.org/articles/13/5335/2020/ doi: 10.5194/amt-13-5335-2020

Grise, K. M., & Polvani, L. M. (2014a). Southern hemisphere cloud–dynamics biases in cmip5 models and their implications for climate projections. *Journal of Climate*, *27*(15), 6074 - 6092. Retrieved from https://journals.ametsoc.org/view/journals/clim/27/15/jcli-d-14-00113.1.xml doi: 10.1175/JCLI-D-14-00113.1

Grise, K. M., & Polvani, L. M. (2014b). Southern hemisphere cloud–dynamics biases in cmip5 models and their implications for climate projections. *Journal of Climate*, *27*(15), 6074 - 6092. Retrieved from https://journals.ametsoc.org/view/journals/clim/27/15/jcli-d-14-00113.1.xml doi: 10.1175/JCLI-D-14-00113.1

Grise, K. M., Polvani, L. M., & Fasullo, J. T. (2015). Reexamining the relationship between climate sensitivity and the southern hemisphere radiation budget in cmip models. *Journal of Climate*, *28*(23), 9298 - 9312. Retrieved from https://journals.ametsoc.org/view/journals/clim/28/23/jcli-d-15-0031.1.xml doi: 10.1175/JCLI-D-15-0031.1

Haynes, J. M., Jakob, C., Rossow, W. B., Tselioudis, G., & Brown, J. (2011). Major characteristics of southern ocean cloud regimes and their effects on the energy budget. *Journal of Climate*, *24*(19), 5061 - 5080. Retrieved from https://journals.ametsoc.org/view/journals/clim/24/19/2011jcli4052.1.xml doi: 10.1175/2011JCLI4052.1

Heese, B., Flentje, H., Althausen, D., Ansmann, A., & Frey, S. (2010). Ceilometer lidar comparison: backscatter coefficient retrieval and signal-to-noise ratio determination. *Atmospheric Measurement Techniques*, *3*(6), 1763–1770. Retrieved from https://amt.copernicus.org/articles/3/1763/2010/ doi: 10.5194/amt-3-1763-2010

Hersbach, H., Bell, B., Berrisford, P., Hirahara, S., Horányi, A., Muñoz-Sabater, J., ... Thépaut, J.-N. (2020). The era5 global reanalysis. *Quarterly Journal of the Royal Meteorological Society*, *146*(730), 1999-2049. Retrieved from https://rmets.onlinelibrary.wiley.com/doi/abs/10.1002/qj.3803 doi: https://doi.org/10.1002/qj.3803

Hoffmann, L., & Spang, R. (2022). An assessment of tropopause characteristics of the era5 and era-interim meteorological reanalyses. *Atmospheric Chemistry and Physics*, *22*(6), 4019–4046. Retrieved from https://acp.copernicus.org/articles/22/4019/2022/ doi: 10.5194/acp-22-4019-2022

Hu, Y., Rodier, S., Xu, K.-M., Sun, W., Huang, J., Lin, B., ... Josset, D. (2010). Occurrence, liquid water content and fraction of supercooled water clouds from combined caliop/iir/modis measurements. *J. Geophys. Res.*, *115*, D00H34.

Huang, Y., Siems, S. T., Manton, M. J., Protat, A., & Delanöe, J. (2012). A study on the low-altitude clouds over the southern ocean using the dardar-mask. *J. Geophys. Res.*, *117*, D18204.

Illingworth, A. J., Hogan, R. J., O'Connor, E., Bouniol, D., Brooks, M. E., Delanoé, J., ... Wrench, C. L. (2007). Cloudnet: Continuous evaluation of cloud profiles in seven operational models using ground-based observations. *B. Am. Meteorol. Soc.*, *88*(6), 883–898. doi: 10.1175/BAMS-88-6-883

ISO 9060:2018. (2018, 11). *Solar energy – Specification of instruments for measuring hemispherical solar and direct solar radiation* (Standard). Geneva, CH: International organization for standardization.

Kanitz, T., Seifert, P., Ansmann, A., Engelmann, R., Althausen, D., Casiccia, C., & Rohwer, E. G. (2011). Contrasting the impact of aerosols at northern and southern midlatitudes on heterogeneous ice formation. *Geophys. Res. Lett.*, *38*(17). doi: 10.1029/2011GL048532

Kay, J. E., Wall, C., Yettella, V., Medeiros, B., Hannay, C., Caldwell, P., & Bitz, C. (2016). Global climate impacts of fixing the southern ocean shortwave radiation bias in the community earth system model (cesm). *Journal of Climate*, *29*(12), 4617 - 4636. Retrieved from `https://journals.ametsoc.org/view/journals/clim/29/12/jcli-d-15-0358.1.xml` doi: 10.1175/JCLI-D-15-0358.1

Komurcu, M., Storelvmo, T., Tan, I., Lohmann, U., Yun, Y., Penner, J. E., ... Takemura, T. (2014). Intercomparison of the cloud water phase among global climate models. *J. Geophys. Res. Atmos.*, *119*(6), 3372–3400. doi: 10.1002/2013jd021119

Küchler, N., Kneifel, S., Löhnert, U., Kollias, P., Czekala, H., & Rose, T. (2017). A w-band radar–radiometer system for accurate and continuous monitoring of clouds and precipitation. *J. Atmos. Oceanic Technol.*, *34*(11), 2375–2392. doi: 10.1175/jtech-d-17-0019.1

Li, Z.-X., & Treut, H. L. (1992). Cloud-radiation feedbacks in a general circulation model and their dependence on cloud modeling assumptions. *Climate Dyn.*, *7*, 133–139.

Mace, G. G., & Protat, A. (2018). Clouds over the southern ocean as observed from the r/v investigator during capricorn. part i: Cloud occurrence and phase partitioning. *Journal of Applied Meteorology and Climatology*, *57*(8), 1783 - 1803. Retrieved from `https://journals.ametsoc.org/view/journals/apme/57/8/jamc-d-17-0194.1.xml` doi: https://doi.org/10.1175/JAMC-D-17-0194.1

Mace, G. G., Protat, A., Humphries, R. S., Alexander, S. P., McRobert, I. M., Ward, J., ... McFarquhar, G. M. (2021). Southern ocean cloud properties derived from capricorn and marcus data. *Journal of Geophysical Research: Atmospheres*, *126*(4), e2020JD033368. Retrieved from `https://agupubs.onlinelibrary.wiley.com/doi/abs/10.1029/2020JD033368` (e2020JD033368 2020JD033368) doi: https://doi.org/10.1029/2020JD033368

McCoy, D. T., Tan, I., Hartmann, D. L., Zelinka, M. D., & Storelvmo, T. (2016). On the relationships among cloud cover, mixed-phase partitioning, and planetary albedo in gcms. *J. Adv. Model. Earth Syst.*, *8*, 650–668.

McFarquhar, G. M., Bretherton, C. S., Marchand, R., Protat, A., DeMott, P. J., Alexander, S. P., ... McDonald, A. (2021). Observations of clouds, aerosols, precipitation, and surface radiation over the southern ocean: An overview of capricorn, marcus, micre, and socrates. *Bulletin of the American Meteorological Society*, *102*(4), E894 - E928. Retrieved from `https://journals.ametsoc.org/view/journals/bams/102/4/BAMS-D-20-0132.1.xml` doi: 10.1175/BAMS-D-20-0132.1

Minnis, P., Sun-Mack, S., Chen, Y., Chang, F., Yost, C. R., Smith, W. L., ... Xie, Y. (2021). Ceres modis cloud product retrievals for edition 4–part i: Algorithm changes. *IEEE Transactions on Geoscience and Remote Sensing*, *59*(4),

2744-2780. doi: 10.1109/TGRS.2020.3008866

Mlawer, E. J., Taubman, S. J., Brown, P. D., Iacono, M. J., & Clough, S. A. (1997). Radiative transfer for inhomogeneous atmospheres: Rrtm, a validated correlated-k model for the longwave. *Journal of Geophysical Research: Atmospheres*, *102*(D14), 16663-16682. Retrieved from https://agupubs.onlinelibrary.wiley.com/doi/abs/10.1029/97JD00237 doi: 10.1029/97JD00237

Mobile radiation observatory (MORDOR). (2022). https://www.tropos.de/en/research/projects-infrastructures-technology/technology-at-tropos/remote-sensing/radiation-measurement-station-bsrn. (Accessed: 2023-02-08)

Morrison, A. E., Siems, S. T., & Manton, M. J. (2011). A three-year climatology of cloud-top phase over the southern ocean and north pacific. *J. Climate*, *24*, 2405–2418.

Mülmenstädt, J., Sourdeval, O., Delanoë, J., & Quaas, J. (2015). Frequency of occurrence of rain from liquid-, mixed-, and ice-phase clouds derived from a-train satellite retrievals. *Geophysical Research Letters*, *42*(15), 6502-6509. Retrieved from https://agupubs.onlinelibrary.wiley.com/doi/abs/10.1002/2015GL064604 doi: https://doi.org/10.1002/2015GL064604

Naud, C., Booth, J. F., & Genio, A. D. D. (2014). Evaluation of era-interim and merra cloudiness in the southern ocean. *J. Climate*, *27*, 2109–2124.

Radenz, M., Bühl, J., Seifert, P., Baars, H., Engelmann, R., Barja González, B., ... Ansmann, A. (2021). Hemispheric contrasts in ice formation in stratiform mixed-phase clouds: disentangling the role of aerosol and dynamics with ground-based remote sensing. *Atmospheric Chemistry and Physics*, *21*(23), 17969–17994. Retrieved from https://acp.copernicus.org/articles/21/17969/2021/ doi: 10.5194/acp-21-17969-2021

Rose, T., Crewell, S., Löhnert, U., & Simmer, C. (2005, may). A network suitable microwave radiometer for operational monitoring of the cloudy atmosphere. *Atmos. Res.*, *75*(3), 183–200. doi: 10.1016/j.atmosres.2004.12.005

Schade, N. H., Macke, A., Sandmann, H., & Stick, C. (2007). Enhanced solar global irradiance during cloudy sky conditions. *Meteorologische Zeitschrift*, 295–303.

Schimmel, W. (2023, March). *Cloudnet products and VOODOO enhancements for a case study of multilayer mixed-phase cloud in Punta Arena Chile.* Zenodo. Retrieved from https://doi.org/10.5281/zenodo.7760395 (We gratefully acknowledge the Federal State of Saxony and the European Social Fund (ESF) in the framework of the programme "Projects in the fields of higher education and research" (grant no. 100339509) and ESF-REACT (grant no. 100602743), and to the Bundesministerium für Bildung und Forschung for the project "Combining MOSAiC and Satellite Observations for Radiative Closure and Climate Implications" (MOSaRiCs) – Project Number 03F0890A.) doi: 10.5281/zenodo.7760395

Schimmel, W., Kalesse-Los, H., Maahn, M., Vogl, T., Foth, A., Garfias, P. S., & Seifert, P. (2022). Identifying cloud droplets beyond lidar attenuation from vertically pointing cloud radar observations using artificial neural networks. *Atmospheric Measurement Techniques*, *15*(18), 5343–5366. Retrieved from https://amt.copernicus.org/articles/15/5343/2022/ doi: 10.5194/amt-15-5343-2022

Shupe, M. D., Uttal, T., & Matrosov, S. Y. (2005). Arctic cloud microphysics retrievals from surface-based remote sensors at sheba. *Journal of Applied Meteorology*, *44*(10), 1544-1562. Retrieved from https://doi.org/10.1175/JAM2297.1 doi: 10.1175/JAM2297.1

Sun, Z., & Shine, K. P. (1994). Studies of the radiative properties of ice and mixed-phase clouds. *Quarterly Journal of the Royal Meteorological Society*, *120*(515), 111-137. Retrieved from https://rmets.onlinelibrary.wiley.com/doi/

abs/10.1002/qj.49712051508 doi: https://doi.org/10.1002/qj.49712051508

Tan, I., & Storelvmo, T. (2019). Evidence of strong contributions from mixed-phase clouds to arctic climate change. *Geophysical Research Letters*, *46*(5), 2894-2902. Retrieved from https://agupubs.onlinelibrary.wiley.com/doi/abs/10.1029/2018GL081871 doi: https://doi.org/10.1029/2018GL081871

Tukiainen, S., O'Connor, E., & Korpinen, A. (2020). Cloudnetpy: A python package for processing cloud remote sensing data. *J. Open Source Softw.*, *5*(53), 2123. doi: 10.21105/joss.02123

Turner, D. D., Shupe, M. D., & Zwink, A. B. (2018). Characteristic atmospheric radiative heating rate profiles in arctic clouds as observed at barrow, alaska. *Journal of Applied Meteorology and Climatology*, *57*(4), 953 - 968. Retrieved from https://journals.ametsoc.org/view/journals/apme/57/4/jamc-d-17-0252.1.xml doi: 10.1175/JAMC-D-17-0252.1

Vergara-Temprado, J., Miltenberger, A. K., Furtado, K., Grosvenor, D. P., Shipway, B. J., Hill, A. A., ... Carslaw, K. S. (2018). Strong control of southern ocean cloud reflectivity by ice-nucleating particles. *Proceedings of the National Academy of Sciences*, *115*(11), 2687-2692. Retrieved from https://www.pnas.org/doi/abs/10.1073/pnas.1721627115 doi: 10.1073/pnas.1721627115

Wang, T., Fetzer, E. J., Wong, S., Kahn, B. H., & Yue, Q. (2016). Validation of modis cloud mask and multilayer flag using cloudsat-calipso cloud profiles and a cross-reference of their cloud classifications. *Journal of Geophysical Research: Atmospheres*, *121*(19), 11,620-11,635. Retrieved from https://agupubs.onlinelibrary.wiley.com/doi/abs/10.1002/2016JD025239 doi: https://doi.org/10.1002/2016JD025239

Witthuhn, J., Hünerbein, A., Filipitsch, F., Wacker, S., Meilinger, S., & Deneke, H. (2021). Aerosol properties and aerosol–radiation interactions in clear sky conditions over germany. *Atmospheric Chemistry and Physics Discussions*, *2021*, 1–64. Retrieved from https://acp.copernicus.org/preprints/acp-2021-517/ doi: 10.5194/acp-2021-517

Xi, B., Dong, X., Zheng, X., & Wu, P. (2022). Cloud phase and macrophysical properties over the southern ocean during the marcus field campaign. *Atmospheric Measurement Techniques*, *15*(12), 3761–3777. Retrieved from https://amt.copernicus.org/articles/15/3761/2022/ doi: 10.5194/amt-15-3761-2022

Zaremba, T. J., Rauber, R. M., McFarquhar, G. M., Hayman, M., Finlon, J. A., & Stechman, D. M. (2020). Phase characterization of cold sector southern ocean cloud tops: Results from socrates. *Journal of Geophysical Research: Atmospheres*, *125*(24), e2020JD033673. Retrieved from https://agupubs.onlinelibrary.wiley.com/doi/abs/10.1029/2020JD033673 (e2020JD033673 2020JD033673) doi: https://doi.org/10.1029/2020JD033673

Zhang, D., Wang, Z., & Liu, D. (2010). A global view of midlevel liquid-layer topped stratiform cloud distribution and phase partition from calipso and cloudsat measurements. *Journal of Geophysical Research: Atmospheres*, *115*(D4). Retrieved from https://agupubs.onlinelibrary.wiley.com/doi/abs/10.1029/2009JD012143 doi: https://doi.org/10.1029/2009JD012143